Chapter 2

Magnetism of Local Moment Systems

The previous chapter introduced a variety of interesting theoretical results concerning the influence of spatial limitations and surfaces on the magnetic behavior. Most of these predictions are connected to changes that should be accessible by experiments. A certain number of experiments confirmed many of these theoretical predictions. However, there is often a major limitation on a clear experimental validation of theory: a real system is usually more complicated than the idealized theoretical model. Therefore, experimentalists are interested in substances that are very close to the theoretical models. Magnetic materials, characterized by strongly localized magnetic moments, represent such model substances. The most prominent local moment elements are the lanthanides. Lanthanide systems are materials with fascinating magnetic properties. The electronic configuration of the lanthanides in the solid state is $[Xe](4f)^n(5d6s)^3$, except for the divalent metals Eu and Yb. This series of elements, shown in Fig. 2.1, is characterized by a successively filling of the $4f$ shell with increasing atomic number. It is almost completely localized within the occupied $5s$ and $5p$ orbitals and remains atomic-like even in the solid state. As a consequence, the $4f$ electrons are not directly involved in the chemical properties of the atoms. The increasing screening of the core potential with the degree of occupancy of the $4f$ shell causes a decrease of the ionic radius. Therefore, the lanthanides are a series of chemically very similar elements that differ by their ionic radius and their magnetic properties. Magnetism arises from the open $4f$ shell, with a systematic variation of spin and orbital moments across the series.

2.1 Lanthanide Metals

Already the elemental metals exhibit a rich variety of magnetic phenomena. While gadolinium (Gd) and divalent europium (Eu) exhibit pure spin magnetism ($L = 0$, $J = S = 7/2$), dysprosium and holmium (Ho) carry the largest total moments of all elements. The direct overlap of the strongly localized $4f$ electrons is a negligible contribution to the inter-atomic coupling, which is rather dominated by the indirect RKKY interaction in the metals [13–15]: This $4f - 4f$ coupling mechanism

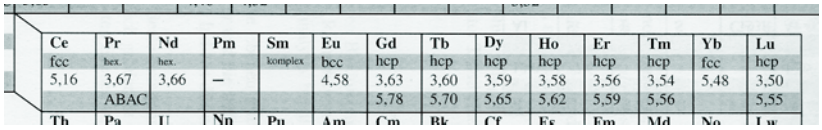

Ce	Pr	Nd	Pm	Sm	Eu	Gd	Tb	Dy	Ho	Er	Tm	Yb	Lu
fcc	hex.	hex.		komplex	bcc	hcp	hcp	hcp	hcp	hcp	hcp	fcc	hcp
5,16	3,67	3,66	–		4,58	3,63	3,60	3,59	3,58	3,56	3,54	5,48	3,50
	ABAC					5,78	5,70	5,65	5,62	5,59	5,56		5,55
Th	Pa	U	Np	Pu	Am	Cm	Bk	Cf	Es	Fm	Md	No	Lw

Figure 2.1: *Excerpt of the periodic system of the elements that shows the series of the lanthanides from Ce to Lu. Displayed properties in the order from top to bottom: symbol of the element, lattice type, lattice parameter a, lattice parameter c. All values are given in Å (from Ref. [71]).*

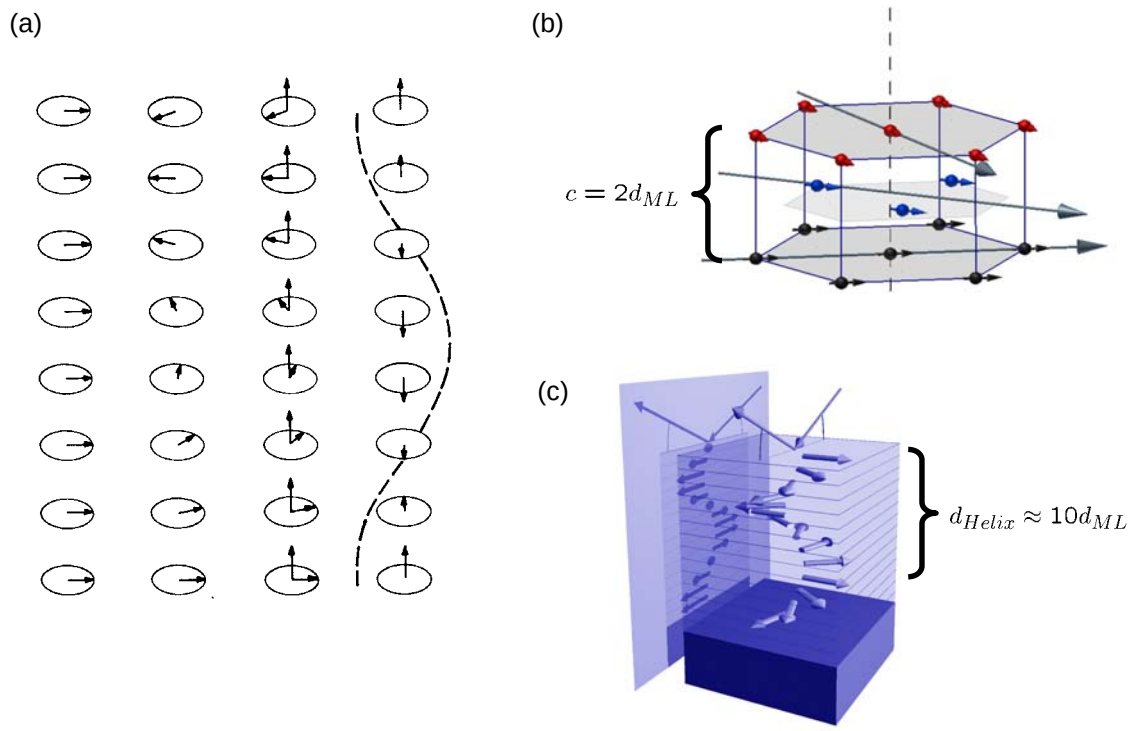

Figure 2.2: *Magnetic structures of the lanthanide metals. (a) Ferromagnet, helical antiferromagnet, conical ferrimagnet, c-axis modulated structure (from left to right) (from Ref. [72]). Right: Chemical and magnetic structure of holmium between 20 K and 132 K. (b) The chemical hexagonal unit cell of holmium metal. In the AFM phase the spins of each close-packed (0001) plane order ferromagnetically, with the magnetization confined to the plane. The magnetization of adjacent layers is rotated, leading to a long-period helical magnetic structure of about ten monolayers along the [0001] direction as shown in (c).*

is due to a direct intra-atomic exchange between the $4f$ electrons and the conduction electrons which then mediate the coupling between the $4f$ electrons of different lattice sites. It is described by the Hamiltonian:

$$H_{ff} = -\frac{1}{2}\sum_{i,j} J_{i,j}^{RKKY} \mathbf{J_i J_j} \quad , \tag{2.1}$$

with $\mathbf{J_i}$,$\mathbf{J_j}$ the total angular momenta of the $4f$ system at the lattice sites i and j. The effective exchange integral $J_{i,j}^{RKKY}$ in the case of isotropic coupling is given by [73]

$$J_{i,j}^{RKKY} \propto g^2 n^{\frac{4}{3}} F\left(2k_F R_{i,j}\right); F(x) = \frac{\sin x - x\cos x}{x^4} \tag{2.2}$$

with k_F the absolute value of the Fermi vector, n the electron density, $R_{i,j}$ the distance of the ions and g quantifying the strength of the intra-atomic coupling to the conduction electrons. The function F shows oscillating behavior and in particular changes its sign periodically with distance (Friedel oscillations). This causes a preference concerning parallel or antiparallel coupling that strongly depends on the distance of two lattice sites. The coupling strength decays with the third power of the distance, which outranges the exponentially decaying direct exchange. This rather long-range coupling mechanism of oscillating sign leads to a rich variety of magnetic structures among the lanthanides that range from simple ferromagnets (Gd) to complex long period helical ferri- and antiferromagnetic

spin arrangements as shown in Fig. 2.2 (a). The almost prototypically localized moments allow for a rather direct comparison with theoretical models such as the Heisenberg lattice.

Besides the ferromagnet Gd, holmium metal is one of the best studied magnetic systems among the lanthanides. It was in particular the subject of one of the first resonant magnetic x-ray scattering experiments [74] with hard x rays and was studied in detail with resonant magnetic soft x-ray scattering at the M_5 threshold [54]. Below the bulk ordering temperature of about 132 K, holmium exhibits a long-period AFM structure that originates from competing FM nearest-neighbor (nn) and AFM next-nearest-neighbor (nnn) interactions. Figure 6.2 (b) displays the hexagonal chemical unit cell of holmium metal. As a consequence of the ABAB stacking sequence the lattice constant c along the [0001] direction is twice the monolayer spacing. The magnetic structure is characterized by FM ordering of the close-packed basal planes with the layer magnetizations confined to these planes. A temperature-dependent turning angle of about 35° of the magnetization directions of adjacent layers leads to the helical magnetic structure along the [0001] direction, depicted in Fig. 2.2 (c). The magnetic period does not match any integer multiple of the monolayer spacing - a so-called incommensurate structure. Below $T_C = 20$ K, a ferrimagnetic cone phase appears that consists of a commensurate helical structure with an out-of-plane component leading to a net magnetic moment along the crystallographic c axis. The fascinating and pronounced magnetic properties of the lanthanides lead to comparably interesting magnetic behavior in a number of lanthanide compounds. One of the most prominent class of magnetic lanthanide compounds are the europium chalcogenides.

2.2 Europium Chalcogenides

The properties of the europium monochalcogenides (EuX, X = O, S, Se, Te) had found interest for the initial hope of technological application of these magnetic semiconducting compounds. While the comparable low ordering temperatures of these materials prevented application so far, they are still of high scientific interest for their prototypical magnetic behavior, evident from a large number of studies in the last decade [75–81]. The magnetism of these divalent semiconductors is caused by the half-filled $4f$ shell of the Eu^{2+} cations with a magnetic ground state ${}^8S_{\frac{7}{2}}$, i.e. ($J = S = 7/2$, $L = 0$) [82]. Thus, these materials show pure spin magnetism due to strongly localized electrons. Along with an almost negligible anisotropy they serve as a prototypical realization of the isotropic Heisenberg model [83]. Within this series of materials (O→Te), the lattice constant increases from 5.14 Å (EuO) to 6.6 Å (EuTe), which permits to study the influence of the ionic distance on magnetism. The increasing lattice constant is accompanied by a decreasing ordering temperature [82] and the occurrence of several different magnetic structures. While EuO and EuS are prototypical Heisenberg ferromagnets, EuTe exhibits AFM order and EuSe shows a so-called metamagnetic behavior characterized by a complicated phase diagram. All of these substances crystallize in the rock-salt structure with the magnetic Eu^{2+} cations forming an fcc sublattice. The magnetic behavior can be described by an isotropic Hamiltonian taking only nn and nnn interactions into account [82]:

$$H = -\sum_{nn} J_1 \mathbf{S_0 S_{nn}} - \sum_{nnn} J_2 \mathbf{S_0 S_{nnn}} \quad . \tag{2.3}$$

Caused by the negligible direct overlap of the $4f$ electrons at different lattice sites and the absence of conduction electrons, the exchange integrals J_1 and J_2 follow from an indirect exchange mechanism. Both couplings involve the $5d$ states of the Eu ions that are split by the crystal field into bonding t_{2g} orbitals pointing towards the nn Eu ion and anti-bonding e_g orbitals along the direction to the neighboring anion (see Fig. 2.3(a)). The ferromagnetic exchange J_1 is called cation-cation-

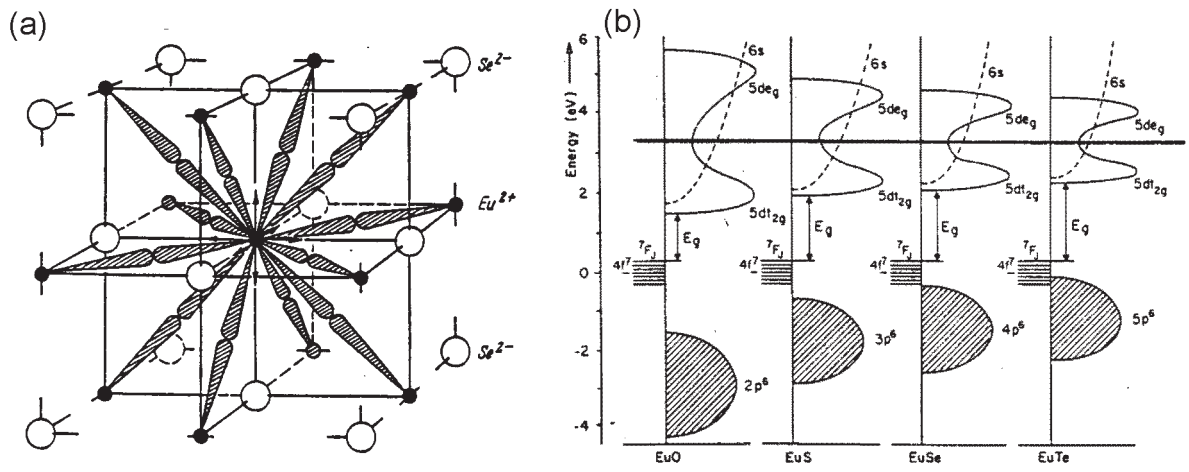

Figure 2.3: *(a) $5d$ orbitals of EuSe. The bonding $5dt_{2g}$ orbitals (hatched) point along the Eu^{2+} nearest neighbor direction (black dots), while the antibonding $5de_g$ orbitals (arrows) are oriented along the cation-anion direction. (b) Schematic electronic band structure of the europium chalcogenides (from Ref. [84]).*

superexchange [82]. This mechanism couples $4f$ moments of neighboring Eu ions via intra atomic $f-d$ exchange and the overlap of the $5dt_{2g}$ orbitals of nn Eu ions. It is described by [82]:

$$J_1 = \frac{t^2 J_{fd}}{2S^2 U^2_{(f-dt_{2g})}} \quad , \tag{2.4}$$

where J_{fd} is the intra atomic exchange of about 0.1 eV, $U_{(f-dt_{2g})}$ the energy difference between $4f^7$ and $5dt_{2g}$ states and t the transfer integral describing essentially the inter atomic overlap. The indirect superexchange that causes J_2 involves the anions. In this case, p electrons of the anions polarize the $4f$ states via overlap of the anion p orbitals and the cation $5de_g$ orbitals by means of intra atomic f-d exchange. This AFM coupling mechanism is quantified by [82]:

$$J_2 = \frac{J^2_{fd}}{U_{(p-de_g)}} \quad , \tag{2.5}$$

with $U_{(p-de_g)}$ is the energy difference between the p and $5de_g$ states. The direct superexchange contributes only to less extent to J_2, but the cross term between both mechanisms turned out to play a decisive role in EuO. Figure 2.3(b) displays schematic electronic band structures of EuX. With increasing size of the anion the band gap E_g between the $4f$ and the $5dt_{2g}$ orbitals strongly increases, while the transfer integral t decreases. This leads to a rapid decay of J_1 with increasing lattice constant. In contrast, the anionic p orbitals slightly shift towards the $5de_g$ orbitals, which results in a weak enhancement of J_2. Hence, the AFM nnn interaction J_2 dominates the behavior of EuTe and leads to a MnO-like (AFM type II) simple antiferromagnetic structure at zero external field[1] below an ordering temperature of 9.8 K as depicted in Fig. 2.4. This structure is characterized by ferromagnetically ordered (111) planes with alternating layer magnetization along the [111] direction. As a consequence, the nn contributions to the total energy cancel for the six in-plane nearest neighbors, which are ferromagnetically aligned, while the three nearest neighbors in each adjacent plane are antiparallel oriented [87]. Thus, the gain in energy due to ordering exclusively originates from the six

[1] In an external magnetic $H > 0.05\ T$, at $T = 9.8$ K, bulk EuTe exhibits a so-called spin-flop or canted phase [85, 86].

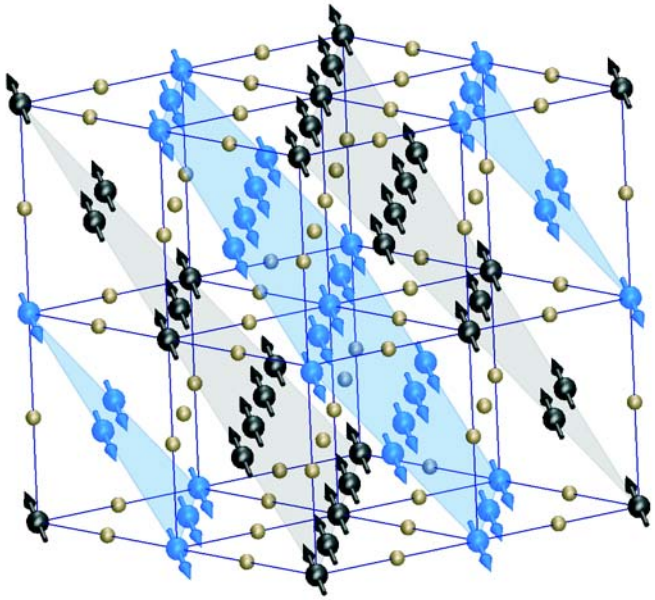

Figure 2.4: *The magnetic unit cell of EuTe. The spins are located at the Eu lattice sites (big spheres), forming an fcc sublattice. The different colors (black and blue) refer to different spin directions. Within the (111) planes (black and blue planes) the moments are ferromagnetically aligned, but with opposite magnetization directions for adjacent planes. The small gray spheres refer to the tellurium lattice sites.*

AFM aligned nnn spins in the two neighboring planes. Despite the fact that the Hamiltonian (Eq. 2.3) is isotropic, it was found that the spins are always confined to the hexagonal planes. This easy-plane anisotropy was accounted for by an additional dipole-dipole interaction [86]. A secondary very weak anisotropy within the plane causes a slight preference for the $[1\bar{1}2]$ direction within the ferromagnetic planes [86]. The four equivalent [111] directions in an ideal crystal give rise to four alternative domains differing in their direction of AFM modulation. These domain types are referred to as T-domains. Experiments on bulk samples revealed that all possible T-domains are populated [88]. For almost a decade, high-quality single-crystalline EuTe(111) samples are available, prepared by means of epitaxial growth on PbTe buffer layers. The simple AFM structure discussed above remains even in samples down to only a few monolayers as proven by neutron scattering experiments [75, 89]. In such thin samples only the T-domain with the modulation direction perpendicular to the surface exists. The scattering experiments suggest that within this T-domain all possible six in-plane domain configurations (six equivalent $[1\bar{1}2]$ easy axes) are equally populated [90]. As a result of the large penetration depth of neutrons, such studies suffer from the comparably weak scattering signal originating from only a few monolayers of EuTe. Therefore, the neutron studies were performed on EuTe/PbTe superlattices consisting of a few hundred periods. As we shall see in the following, resonant magnetic soft x-ray diffraction offers a unique tool to study even single ultra-thin magnetic layers.